Experimental and numerical observation of dark and bright breathers in the band gap of a diatomic electrical lattice

F. Palmero,[1] L. Q. English,[2] Xuan-Lin Chen,[3] Weilun Li,[2] Jesús Cuevas-Maraver,[4] and P. G. Kevrekidis[5]

[1]*Grupo de Física No Lineal, Departamento de Física Aplicada I, Escuela Técnica Superior de Ingeniería Informática, Universidad de Sevilla, Avda Reina Mercedes s/n, E-41012 Sevilla, Spain*

[2]*Department of Physics and Astronomy, Dickinson College, Carlisle, Pennsylvania 17013, USA*

[3]*Physics Department, Harbin Institute of Technology, Harbin 150001, Heilongjiang Province, China*

[4]*Grupo de Física No Lineal, Departamento de Física Aplicada I, Escuela Politécnica Superior, Universidad de Sevilla, Virgen de África 7, 41011 Sevilla, Spain and Instituto de Matemáticas de la Universidad de Sevilla (IMUS), Edificio Celestino Mutis, Avda Reina Mercedes s/n, E-41012 Sevilla, Spain*

[5]*Department of Mathematics and Statistics, University of Massachusetts, Amherst, Massachusetts 01003, USA*

(Received 11 November 2018; published 7 March 2019)

We observe dark and bright intrinsic localized modes (ILMs), also known as discrete breathers, experimentally and numerically in a diatomic-like electrical lattice. The experimental generation of dark ILMs by driving a dissipative lattice with spatially homogenous amplitude is, to our knowledge, unprecedented. In addition, the experimental manifestation of bright breathers within the band gap is also novel in this system. In experimental measurements the dark modes appear just below the bottom of the top branch in frequency. As the frequency is then lowered further into the band gap, the dark ILMs persist, until the nonlinear localization pattern reverses and bright ILMs appear on top of the finite background. Deep into the band gap, only a single bright structure survives in a lattice of 32 nodes. The vicinity of the bottom band also features bright and dark self-localized excitations. These results pave the way for a more systematic study of dark breathers and their bifurcations in diatomic-like chains.

DOI: 10.1103/PhysRevE.99.032206

I. INTRODUCTION

The study of intrinsic localized modes (ILMs) was arguably initiated by the Refs. [1,2] on the so-called Fermi-Pasta-Ulam-Tsingou lattices. It was subsequently significantly propelled forward by the rigorous proof of their existence in a large class of models starting from the uncoupled, so-called anticontinuous limit [3]. Since then, there has been a wide variety of systems in which experimental observations of structures have been reported that are exponentially localized in space and periodic in time. Among them, one can note arrays of Josephson junctions [4,5], mechanical [6,7] and magnetic pendula [8], microcantilevers [9], electrical chains [10,11], granular crystals, [12,13], ionic crystals such as PtCl [14], and antiferromagnets [15]. Moreover, these types of structures have been offered as plausible explantions of experimental findings in settings such as the DNA denaturation [16], α-uranium [17], or NaI [18]. For relevant reviews of ILMs, see, e.g., Refs. [19–21], as well as the more specialized works regarding optical [22] atomic [23] and solid-state physics [24] applications and books such as Ref. [25].

A significant early playground for the exploration of ILMs has been offered by the setting of electrical lattices [26]. Progressively, since the late 2000s, these lattices have enjoyed a larger degree of control of their external drive and lattice configurations (one- vs. two-dimensional, nearest- vs. beyond-nearest-neighbor configurations, etc.) [10,27–29]. In these works, a qualitatively and semiquantitatively accurate model of the dynamics has also been put forth. Building on this existing experimental, theoretical, and computational background, we now advance a diatomic-like electrical lattice model.

More specifically, we construct a coupled-resonator circuit where one of the inductive elements alternates between two values for adjacent nodes, endowing the lattice with a diatomic structure. Such electrical lattices have been proposed (and even experimentally explored) since the early days of localized dynamics; see, e.g., Ref. [30]. Here, however, we explore some features not previously discussed, to the best of our knowledge. After confirming the linear two-band spectrum, we search the band gap for the existence of nonlinear excitations. Both in the experiment and in the numerical simulations of the model, we identify breather structures consisting of density dips in a finite background, namely the so-called dark breathers (DBs). To the best of our knowledge, such DBs have previously been induced experimentally only in granular crystals [13] on the basis of earlier theoretical predictions in Hamiltonian and dissipative lattices, such as Refs. [31,32]. Nevertheless, the latter setting only affords control of the driving boundaries, while no drive or spatiotemporal controls are available within the chain, as is the case herein. Hence, it can be argued that the present setting is far more amenable to the controllable generation and persistence of these states. DBs are found in the vicinity of the top band and, as we drive deeper into the spectral gap, the nonlinear states sustain a fundamental change of character and become bright ones, on top of the finite background (which previously supported the DBs). In addition, we have found that below the bottom band

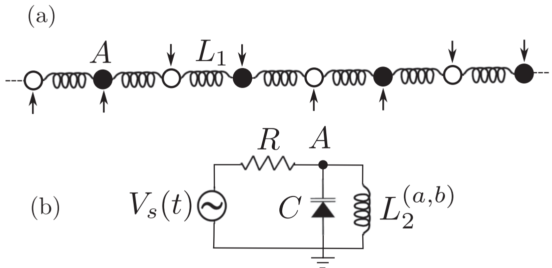

FIG. 1. (a) Schematic circuit diagrams of the electrical lattice, where the blank points represents circuit cells of type (a) and black points represent circuit cells of type (b). Black arrows represent driving and its phase. (b) Each cell is connected to a periodic voltage source $V_s(t)$ via a resistor R and grounded. Each point A of an elemental circuit is connected via inductors L_1 to the corresponding points A of neighboring cell. Voltages are monitored at point A.

the system features dark and bright ILMs structures as well. To the best of our knowledge, such features are unprecedented in electrical chains or, for that matter, in experimentally tractable nonlinear dynamical lattices generally.

Our presentation is structured as follows. First, we present the experimental setup and corresponding theoretical model. We then discuss our results for both dark and bright ILMs. Finally, we summarize our findings and present some directions for future study.

II. EXPERIMENTAL AND THEORETICAL SETUP

In our electrical lattice, the connected nodes are RLC resonators comprised of inductors $L_2^{(a,b)}$ and varactor diodes providing a voltage-dependent, nonlinear capacitance, $C(V)$. In order to make this lattice a diatomic system, we have incorporated two different cells, (a) and (b), with different values of inductors, $L_2^{(a)}$ and $L_2^{(b)}$, located on alternate sites. Thus, the unit cell is the node pair, and each node of one type is surrounded by two nodes of the other type. Neighboring nodes are coupled inductively via inductors, L_1, and driven by a sinusoidal signal via a resistor, R. We also connect the last circuit cell to the first, thus implementing periodic boundary conditions.

The sinusoidal driver is spatially homogenous in amplitude but staggered in space from one unit cell to the next. This drive was provided by an Agilent 33220A function generator, which for half the nodes was inverted using a fast operational amplifier (LF411). The integrity of the signals was checked with an oscilloscope. This means that we instituted a phase shift of π between two consecutive nodes of the same type, so that the zone boundary plane-wave modes could be excited. (The two sites within a given unit cell were driven in phase.) We denote the driver amplitude by V_d and its angular frequency by ω_d. A sketch of the system is shown in Fig. 1.

Furthermore, the concrete parameter values of the system (composed of inductors, resistors, and capacitors) are $L_1 = 0.68$ mH, $L_2^{(a)} = 102.7$ μH, $L_2^{(b)} = 970$ μH, $R = 10$ kΩ and the capacitance at zero voltage of the varactor (NTE 618) is $C_0 = 770$ pF. The number of nodes of each type was $N^{(a)} = N^{(b)} = 16$, equaling 16 unit cells for a total of 32 nodes. Experimentally, node voltages V_n at points A were measured at a rate of 2.5 MHz using a 32-channel analog-to-digital converter. In order to obtain a higher-resolution picture of the nonlinear localized modes, the full time-series experimental data (of around 100 driver periods) can be folded back into a single period using knowledge of the precise temporal periodicity (i.e., frequency). These higher-resolution pictures also compare very well to traces independently taken at individual nodes with a 1-GS/s oscilloscope.

We should note that a macroscopic lattice can never be made exactly homogeneous from node to node, but the inhomogeneity in our electrical lattice is small. More precisely, all inductors used bear inductances to within 1% of one another, and the varactor diodes have a standard deviation in their measured capacitance of about 3%. Their exact nonlinear response cannot be captured by a single number, of course, but we would expect these p-n junctions to behave very much alike. The relative insignificance of the lattice inhomogeneity can be demonstrated by observing that ILMs can be created anywhere in the lattice.

It has been shown that the basic dynamics of this electrical network can be qualitatively described by a simple model where the introduction of an amplitude-dependent phenomenological resistor, R_l, in parallel to the cell capacitance, is enough to reproduce experimentally observed features quite well [10]. Accordingly, the dimensionless equations of motion read

$$\begin{aligned} \frac{di_n}{d\tau} &= \frac{L_2^{(a)}}{L_1}(v_{n+1} + v_{n-1} - 2v_n) - \frac{L_2^{(a)}}{L_2^{(n)}} v_n \\ \frac{dv_n}{d\tau} &= \frac{1}{c(v_n)}\left[i - i_d + \frac{\cos(\Omega\tau)}{\omega_0 R C_0} - \frac{v_n}{\omega_0 R_e C_0}\right], \end{aligned} \tag{1}$$

where $L_2^{(n)} = L_2^{(a)}$ if site (n) corresponds to nodes (a) or $L_2^{(n)} = L_2^{(b)}$ if it corresponds to nodes (b). The following dimensionless variables have been used: $\tau = \omega_0 t$; $i_n = (I_v - I_2)/(\omega_0 C_0 V_d)$, where I_v is the full current through the unit cell and I_2 is the current through the inductor $L_2^{(n)}$, both corresponding to cell n; $v_n = V_n/V_d$. Here V_d is the driver amplitude, and V_n is the measured voltage at node n; $\Omega = \omega_d/\omega_0$, $\omega_0 = 1/\sqrt{L_2^{(a)} C_0}$; $i_d = I_D/(\omega_0 C_0 V_d)$, where I_D is the current through the varactor diode; $c = C(V)/C_0$, and $C(V)$ is the nonlinear capacitance of the diode. R_e is the equivalent resistance so $1/R_e = 1/R + 1/R_l$.

The main loss/decay channels in this experimental system are the varactor diodes during the negative voltage swings (forward bias) due to resistive current flow and recombination effects. In addition to this on-site dissipative channel, the coupling inductors also have some series resistance which gives rise to a small intersite resistance. The model ignores these details in favor of only one phenomenological term, R_l.

Numerically we have calculated discrete breathers as spatially localized periodic solutions of Eq. (1). In order to study their linear stability we have examined the evolution of a small perturbation of a given periodic solution to first order and performed a Floquet analysis. ILM stability is then determined by the Floquet multipliers so that if the coherent structure is stable, then all of them lie inside the unit circle [10,33].

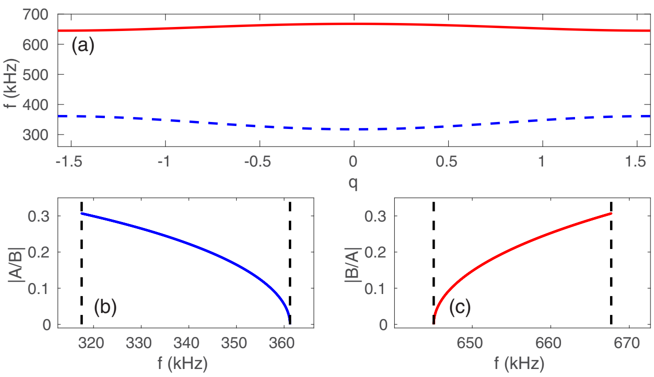

FIG. 2. (a) Electrical line linear mode frequencies f as function of the wave vector $q = n\pi/N$, where $n = -N/2 \dots N/2$ and $N = N^{(a)} + N^{(b)}$, where $N^{(a)}$ is the number of cells of type (a), and likewise for (b). A solid (dashed) line is used to denote the upper (lower) band. Panels (b) and (c) show the ratios between different linear mode amplitudes in the bands, where A correspond to oscillation amplitudes of cells of type (a) and B to cells of type (b).

III. RESULTS AND DISCUSSION

In the limit of no driving and for small-amplitude oscillations the linear modes possess frequencies grouped into two bands, as expected on the basis of the diatomic structure of the lattice. The upper (optic-like) and lower (acoustic-like) bands of the linear spectrum are found to lie within the intervals 314–356 and 645–666 kHz, respectively. A plot of the theoretical dispersion bands—obtained from linearizing Eq. (1)—is shown in Fig. 2, and the linear modes corresponding to top and bottom of the two bands are shown in Fig. 3. Using the spatial signature of the driving outlined before, we are able to experimentally excite and pump the linear mode of Figs. 3(c) and 3(b), and we proceed to explore the dynamics of such a mode for frequencies within the band gap (i.e., in the regime of nonlinear, breatherlike excitations [20]).

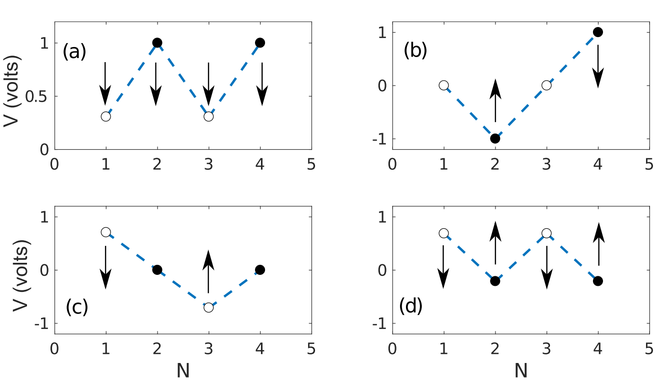

FIG. 3. Sketch of the linear modes corresponding to the top and the bottom of the bands shown in Fig. 2. (a) Uniform linear mode corresponding to the bottom of the lower band. (b) Linear mode corresponding to the top of the lower band, where the $L_2^{(b)}$ sublattice oscillates out of phase and the other sublattice is at rest. (c) Linear mode corresponding to the bottom of the upper band, where the $L_2^{(a)}$ sublattice oscillates out of phase, and the other sublattice is at rest. (d) Linear mode corresponding to the top of the upper band, where all neighboring cells oscillate out of phase.

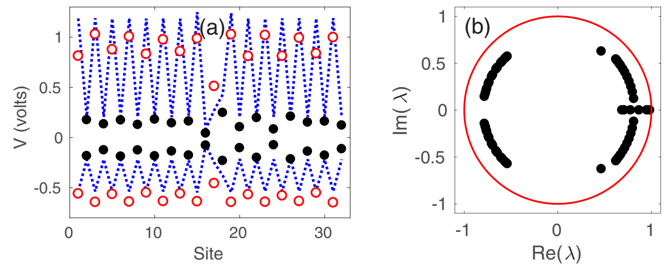

FIG. 4. (a) Numerical (dotted line) and experimental (circles) DB profile (maximum and minimum amplitude) corresponding to $V_d = 3.5$ V and $f = 571$ kHz. Blank points represent circuit cells of type (a) and black points represent circuit cells of type (b). (b) Floquet multiplier numerical linearization spectrum confirming that, since all multipliers are inside the unit circle, the solution is stable.

A. Dark gap breathers

The existence of bright ILMs below the lower linear dispersion band has been well established in such systems, driven either directly or with a subharmonic driver [10,27–29]. In this work, we focus on the existence and properties of ILMs in the band gap, where we have, remarkably, found both dark and bright breathers (with nonvanishing background), depending on the precise driver frequency within the gap.

Figure 4 shows the experimental result for driving at a frequency of 571 kHz, about 25% into the gap from above and 74 kHz below the bottom of the upper band (the zone-boundary mode is at 645 kHz). The amplitude is $V_d = 3.5$ V. The lattice profile of maximum and minimum node voltages in Fig. 4 clearly indicates the presence of a dark localized mode located around nodes 16 and 17. The term "dark" is used to describe a localized mode for which the amplitude of oscillation is large and constant in the lattice except at the ILM center and in its close vicinity (where it is near vanishing). Such structures, although theoretically proposed early in Ref. [32], were only identified quite recently in a materials system (a granular crystal) in Ref. [12]. There they were produced as a result of the destructive interference of waves emanating from the boundary, while here they are robustly created by the drive within the band gap, as evidenced in the computational stability analysis of Fig. 4. Figure 5 shows the experimental and numerical time series at selected nodes. On one sublattice,

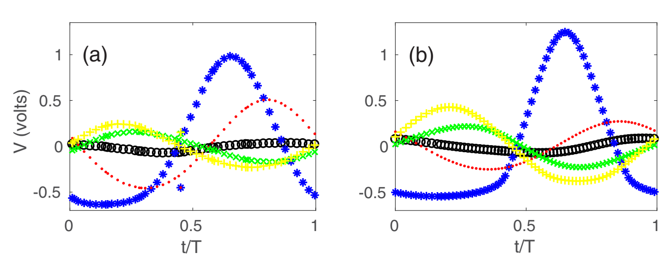

FIG. 5. (a) Experimental and (b) numerical voltage oscillations of the DB corresponding to $V_d = 3.5$ V and $f = 571$ kHz: site 16 (black circles), first-neighbor sites 15 (blue diamond), and 17 (red dots), and second neighbors: sites 14 (green crosses) and 18 (yellow pluses).

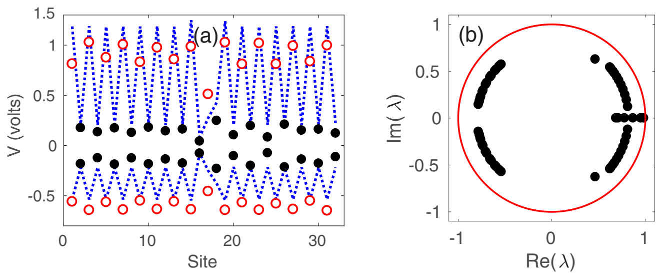

FIG. 6. (a) Numerical (dotted line) and experimental (circles) three–peak DB profile (maximum and minimum amplitude) corresponding to $V_d = 3.5$ V and $f = 567$ kHz. Blank points represent circuit cells of type (a) and black points represent circuit cells of type (b). (b) Floquet multiplier numerical linearization spectrum confirming the stability of the solution since all multipliers are inside the unit circle.

node 17 (red dots) is suppressed relative to node 15 (blue diamonds), and on the other sublattice, node 16 (black, open circle) is suppressed relative to nodes 14 (green crosses) and 18 (yellow pluses). Experimentally (left panel), we see that the amplitude on the large-oscillation sublattice is reduced at the dark ILM center to about half the value in the wings. Numerically (right panel) the reduction is similarly (or even more) pronounced for these particular driving conditions.

In other experimental runs, the center of the dark ILM forms at different locations within the lattice, so this is not an impurity effect and as expected in a longer (nearly) homogeneous lattice the DB enjoys the discrete shift invariance of the diatomic chain. Nevertheless, we also observe that the the location can be predetermined (i.e., designed) by placing a temporary impurity at the chosen site before turning on the driver. The sign of the impurity necessary to seed a dark ILM is opposite to the one needed for bright ILMs. Numerically, we find stable one-peak DBs existing in the range of 569.5–600 kHz for a drive amplitude of $V_d = 3.5$ V. It remains an important, albeit numerically rather demanding, question as to whether the DB can be found in computations throughout the system's band gap.

Decreasing the driving frequency further into the band gap, a pattern of multipeak dark ILMs emerges, as shown in Fig. 6. The number of dark ILMs in the lattice is very sensitive to the precise driver frequency at constant amplitude. In general, decreasing the driving frequency produces multipeak structures and numerical solutions show overall good agreement with experimental results. However, numerics and experiments differ as to the precise localization centers, and in experiments they are found to be spaced somewhat more closely than in the numerical results. Nevertheless, the numerical results strongly suggest that such coherent structures should be dynamically robust, in line with the corresponding experimental observations. As also seen in previous studies, where the ILM is generated by a uniform driver, it can be sensitive to small lattice impurities which are, unfortunately, hard to completely eliminate in a manufactured lattice.

B. Bright gap breathers

As we have seen, on lowering the frequency, the DBs persist and apparently the number of their stable dips is

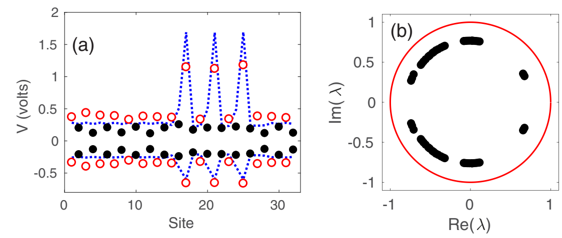

FIG. 7. (a) Numerical (dotted line) and experimental (circles) three-peak bright breather profile (maximum and minimum amplitude) corresponding to $V_d = 3.5$ V and $f = 532$ kHz. Blank points represent circuit cells of type (a) and black points represent circuit cells of type (b). (b) Floquet multiplier numerical linearization spectrum confirming the stability of the solution.

increased within the chain. It is interesting that this is analogous to the phenomenology observed in the granular case, as discussed in Ref. [12]. Nevertheless, as the frequency is further reduced, an unprecedented (to our knowledge) scenario develops. More specifically, the localized pattern inverts, i.e., an excited set of nodes appears above the background value. Thus, a train of bright localized modes appears. If the frequency is further lowered within the gap, then the peaks within this multipeak pattern become more sparse until finally only a single such bright breather survives. Below this lower threshold, the driver cannot sustain any lattice modes at the given driving amplitude—linear or nonlinear—until we get into the vicinity of the bottom band. For an amplitude of 3.5 V, the experimental threshold lies at 528 kHz, well above the upper edge of the bottom band.

Figures 7 and 8 depict these bright localized modes for two different drive frequencies, separated by 4 kHz. At the higher frequency, three ILMs survive, whereas at 528 kHz, we are left with a single bright breather. Let us briefly examine the spatial structure of this state. Its center always resides on the $L_2^{(a)}$ sublattice, namely on a cell with lower inductance, L_2. Further, these breathers are extremely sharp—the nearest neighbors on the $L_2^{(b)}$ sublattice register a slightly larger oscillation amplitude compared to the wings, but beyond that no increase beyond background can be discerned. The background oscillation is characterized by the $L_2^{(b)}$ sublattice almost at rest, undergoing only small oscillations, whereas

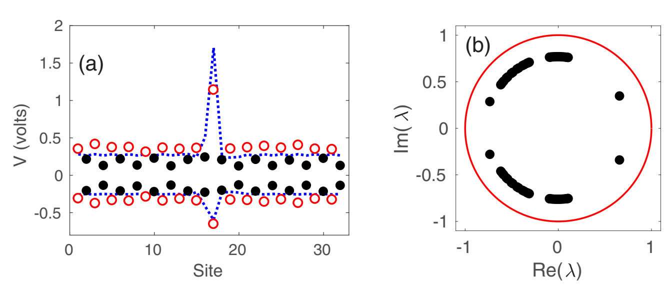

FIG. 8. (a) Numerical (dotted line) and experimental (circles) one-peak bright breather profile (maximum and minimum amplitude) corresponding to $V_d = 3.5$ V and $f = 528$ kHz. Blank points represent circuit cells of type (a) and black points represent circuit cells of type (b). (b) Floquet multiplier numerical linearization spectrum confirming, similarly as above, the stability of the solution.

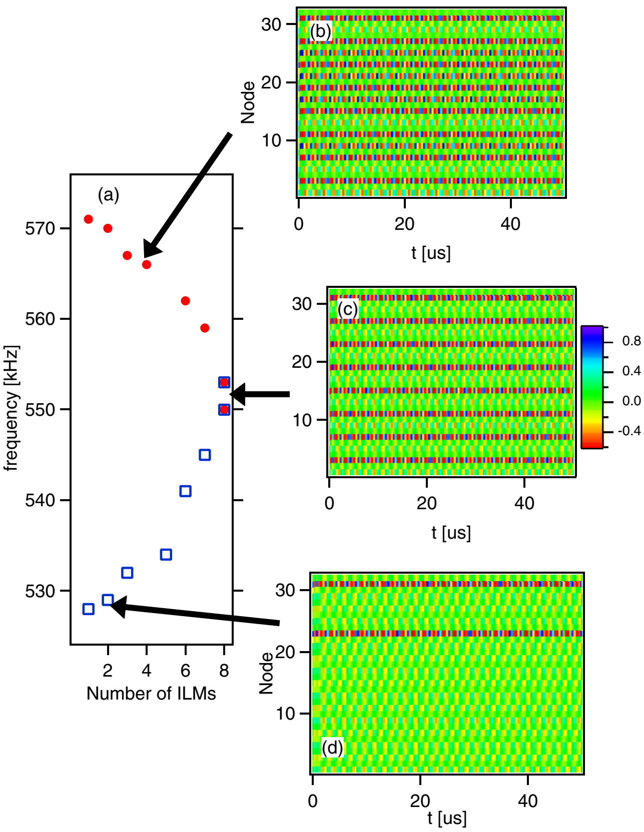

FIG. 9. Summary of the progression from dark to bright multipeak ILM structures. Panels (a) show the driver frequency as a function of the number of breathers, both dark (circles, red) and bright (squares, blue). At around 550 kHz, we observe an equal mixture of bright and dark breathers. Panels (b)–(d) show the experimental data corresponding to select frequencies.

the $L_2^{(a)}$ sublattice is oscillating out of phase. Thus, the ILM wings, or background, is consistent with the top (i.e., optic) zone-boundary mode pattern. These observations are in good agreement with numerical results. The precise width of any stability region is hard to match because there exist regions of different peak numbers and regions of different families with the same number of peaks that all overlap.

Figure 9(a) effectively summarizes the experimental picture and thus yields a first clue to the kind of bifurcation diagram mentioned above. In particular, it depicts the transition from dark to bright breathers as the frequency is lowered starting closer to the bottom of the upper band and moving progressively deeper into the band gap. At the highest frequency considered within the gap, the zone-boundary plane-wave mode is excited at high amplitude. As the frequency is somewhat lowered, first a single DB and then multipeak DBs are generated. Then, as the frequency is further lowered into the band gap, eventually a striped nonlinear pattern is seen [Fig. 9(c)], which could also be characterized as a (roughly) equal mixture of bright and dark breathers. Below that frequency, we observe bright breathers, whose numbers in the lattice decrease as the drive frequency is further lowered. It is worth noting that the bright breathers, when multiple of them arise, are found to always be in phase.

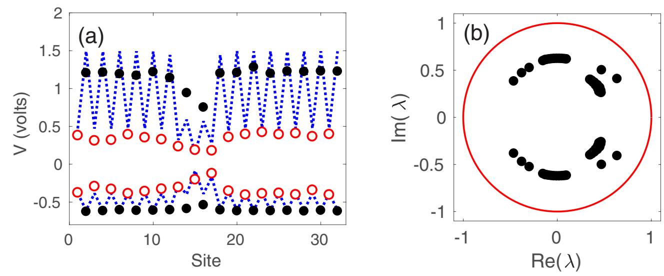

FIG. 10. (a) Numerical (dotted line) and experimental (circles) DB profile (maximum and minimum amplitude) corresponding to $V_d = 3.5$ V and $f = 280$ kHz. Blank points represent circuit cells of type (a) and black points represent circuit cells of type (b). (b) Floquet multiplier numerical linearization spectrum confirming the stability of the solution.

The supporting panels, Figs. 9(b)–9(d), depict the experimental data in time and space at select drive frequencies. This is one of the especially appealing aspects of this system, namely the ability for distributed characterization/visualization of the dynamics (in addition to the distributed driving capabilities for this system). Note that the pattern characterizing equal numbers of bright and dark ILMs is qualitatively different from the nonlinear zone-boundary mode. In fact, its spatial periodicity is doubled, and one could describe the resulting pattern as a dynamically induced superlattice. We also note that while the DBs are sharply localized in this system (as are the bright ones), they do encompass several lattice nodes. Finally, the DBs can be shepherded spatially via temporarily induced impurities at neighboring sites. The experimentally easiest way to do this is to alter the effective inductance of the inductor L_2. Whereas bright breathers are attracted to a neighboring site of higher L_2, the opposite is the case for DBs; they are attracted to a site with lower L_2. This tunability can be important for the controllable transfer of energy within such a system.

C. Near the bottom band

The vicinity of the bottom band also features bright and dark ILMs. Figure 10 depicts the situation at a driver frequency of 280 kHz, just below the bottom of the band. One DB is clearly visible at site $n = 13$ in the experimental data. Simulations also find this DB, although the background amplitude is slightly higher than in the experiment under identical driving conditions. Floquet analysis again shows that this mode is dynamically stable; see Fig. 10(b).

If the driving frequency is lowered by a mere 10 kHz to 270 kHz, then bright ILMs are generated. These bright ILMs just below the bottom band are different from the bright ILMs of the top band in that their localization centers are on the opposite sublattice, namely the sublattice of $L_2^{(b)}$ sites characterized by the larger inductance value. The situation is succinctly depicted in Fig. 11 where so-called *frequency shift key* modulation (FSK) is employed to switch the driver frequency abruptly from one value to another. Here a shift from 271 to 543 kHz was initiated in the experiment at a time of 2000 μs. The first frequency is consistent with two bright breathers with the associated (lower) frequency, whereas the

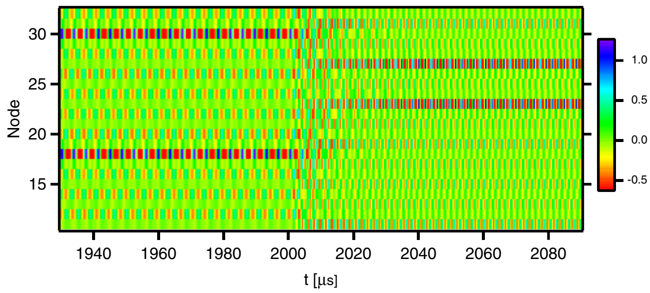

FIG. 11. Experimental FSK modulation that switches abruptly between two distinct values of the driving frequency while keeping the amplitude fixed at 3.5 V. Initially, for $f = 271$ kHz, two breathers are seen, but then when the frequency switches to 543 kHz, two distinct ILMs at a different location with the latter frequency (centered on odd sites) develop.

second generates two bright breathers with the corresponding (higher) frequency in a different location. We see that the breathers are initially located on even sites, but after 2000 μs quickly settle on odd sites. The FSK technique can also be used to switch between bright and dark breathers within the upper band, by selecting two appropriate drive frequencies, such as 565 and 535 kHz.

IV. CONCLUSIONS AND FUTURE WORK

In the present work, we have examined the setting of electrical lattices in the form of a controllable/tunable diatomic-like system. Building on the modeling successfully used earlier for the monatomic case, we have considered both the linear and especially the nonlinear properties of this system, examining them in parallel both at the experimental and numerical level. We have found these lattices to be very useful playgrounds for the exploration of dark breather and multibreather structures. Such states have spontaneously emerged in the experiments at different frequencies within the band gap near the top band. However, as one further lowers the frequency, a bright nonlinear structure (on top of a background) emerged, involving initially multiple peaks, which then become progressively fewer (as the frequency was further lowered), before eventually disappearing altogether well above the cutoff frequency of the bottom band.

While the structures reported here, we feel, are intriguing, they also pose numerous open questions for future consideration. Many of these can be addressed by a systematic analysis of the bifurcations of single and multiple dark and bright breathers in the band gap. Such an analysis, while computationally demanding, would offer a more systematic roadmap for future experiments. There we could explore what happens in the immediate vicinity of the (upper edge of the) bottom branch, as well as the (lower edge of the) top branch. Extensions of these fairly controllable structures would also be worthwhile to consider in higher-dimensional systems. Some of these questions are currently under consideration and will be reported in future publications.

ACKNOWLEDGMENTS

F. Palmero visited Dickinson College with support from the VI Plan Propio of the University of Seville (VI PPIT-US). X.-L. Chen was also at Dickinson College for part of this study. This material is based on work supported by the National Science Foundation under Grant No. PHY-1602994 and Grant No. DMS-1809074 and the US-AFOSR via Grant No. FA9550-17-1-0114. J.C.-M. was supported by MAT2016-79866-R project (AEI/FEDER, UE).

[1] A. J. Sievers and S. Takeno, Phys. Rev. Lett. **61**, 970 (1988).
[2] S. Takeno, K. Kisoda, and A. J. Sievers, Prog. Theor. Phys. Suppl. **94**, 242 (1988).
[3] R. S. MacKay and S. Aubry, Nonlinearity **7**, 1623 (1994).
[4] E. Trías, J. J. Mazo, and T. P. Orlando, Phys. Rev. Lett. **84**, 741 (2000).
[5] P. Binder, D. Abraimov, A. V. Ustinov, S. Flach, and Y. Zolotaryuk, Phys. Rev. Lett. **84**, 745 (2000).
[6] J. Cuevas, L. Q. English, P. G. Kevrekidis, and M. Anderson, Phys. Rev. Lett. **102**, 224101 (2009).
[7] F. Palmero, J. Han, L. Q. English, T. J. Alexander, and P. G. Kevrekidis, Phys. Lett. A **380**, 401 (2016).
[8] F. M. Russell, Y. Zolotaryuk, J. C. Eilbeck, and T. Dauxois, Phys. Rev. B **55**, 6304 (1997).
[9] M. Sato, B. E. Hubbard, and A. J. Sievers, Rev. Mod. Phys. **78**, 137 (2006).
[10] F. Palmero, L. Q. English, J. Cuevas, R. Carretero-González, and P. G. Kevrekidis, Phys. Rev. E **84**, 026605 (2011).
[11] L. Q. English, F. Palmero, J. F. Stormes, J. Cuevas, R. Carretero-González, and P. G. Kevrekidis, Phys. Rev. E **88**, 022912 (2013).
[12] N. Boechler, G. Theocharis, S. Job, P. G. Kevrekidis, Mason A. Porter, and C. Daraio, Phys. Rev. Lett. **104**, 244302 (2010).
[13] C. Chong, F. Li, J. Yang, M. O. Williams, I. G. Kevrekidis, P. G. Kevrekidis, and C. Daraio, Phys. Rev. E **89**, 032924 (2014).
[14] B. I. Swanson, J. A. Brozik, S. P. Love, G. F. Strouse, A. P. Shreve, A. R. Bishop, W.-Z. Wang, and M. I. Salkola, Phys. Rev. Lett. **82**, 3288 (1999).
[15] M. Sato and A. J. Sievers, Nature **432**, 486 (2004).
[16] M. Peyrard, Nonlinearity **17**, R1 (2004).
[17] M. E. Manley, M. Yethiraj, H. Sinn, H. M. Volz, A. Alatas, J. C. Lashley, W. L. Hults, G. H. Lander, and J. L. Smith, Phys. Rev. Lett. **96**, 125501 (2006).
[18] M. E. Manley, A. J. Sievers, J. W. Lynn, S. A. Kiselev, N. I. Agladze, Y. Chen, A. Llobet, and A. Alatas, Phys. Rev. B **79**, 134304 (2009).
[19] S. Flach and C. R. Willis, Phys. Rep. **295**, 181 (1998).
[20] S. Flach and A. V. Gorbach, Phys. Rep. **467**, 1 (2008).
[21] S. Aubry, Physica D **216**, 1 (2006).
[22] F. Lederer, G. I. Stegeman, D. N. Christodoulides, G. Assanto, M. Segev, and Y. Silberberg, Phys. Rep. **463**, 1 (2008).
[23] O. Morsch and M. Oberthaler, Rev. Mod. Phys. **78**, 179 (2006).

[24] S. V. Dmitriev, E. A. Korznikova, Yu. A. Baimova, and M. G. Velarde, Phys.-Uspekhi **59**, 446 (2016).

[25] T. Dauxois and M. Peyrard, *Physics of Solitons* (Cambridge University Press, Cambridge, 2006); J. F. R. Archilla, N. Jiménez, V. J. Sánchez-Morcillo, and L. M. García-Raffi (eds.), *Quodons in Mica: Nonlinear Travelling Excitations in Crystals* (Springer, Cham, 2015).

[26] M. Remoissenet, *Waves Called Solitons* (Springer-Verlag, New York, 1999).

[27] L. Q. English, F. Palmero, P. Candiani, J. Cuevas, R. Carretero-Gonzalez, P. G. Kevrekidis, and A. J. Sievers, Phys. Rev. Lett. **108**, 084101 (2012).

[28] M. Sato, S. Yasui, M. Kimura, T. Hikihara, and A. J. Sievers, Europhys. Lett. **80**, 30002 (2007).

[29] L. Q. English, R. B. Thakur, and R. Stearrett, Phys. Rev. E **77**, 066601 (2008).

[30] T. Kofane, B. Michaux, and M. Remoissenet, J. Phys. C: Solid State Phys. **21**, 1395 (1988).

[31] A. Álvarez, J. F. R. Archilla, J. Cuevas, and F. R. Romero, New J. Phys. **4**, 1 (2002).

[32] B. Sánchez-Rey, G. James, J. Cuevas, and J. F. R. Archilla, Phys. Rev. B **70**, 014301 (2004).

[33] J. L. Marìn, F. Falo, P. J. Martínez, and L. M. Floría, Phys. Rev. E **63**, 066603 (2001).